Geoscience Frontiers 12 (2021) 101229

HOSTED BY

Contents lists available at ScienceDirect

Geoscience Frontiers

journal homepage: www.elsevier.com/locate/gsf

Research Paper

A sensitivity study of the WRF model in offshore wind modeling over the Baltic Sea

Huidong Li [a,*], Björn Claremar [a], Lichuan Wu [a], Christoffer Hallgren [a], Heiner Körnich [b], Stefan Ivanell [a], Erik Sahlée [a]

[a] Department of Earth Sciences, Uppsala University, Uppsala 75236, Sweden
[b] Swedish Meteorological and Hydrological Institute, Norrköping 60176, Sweden

ARTICLE INFO

Article history:
Received 11 March 2021
Revised 1 May 2021
Accepted 14 May 2021
Available online 20 May 2021
Handling Editor: M. Santosh

Keywords:
Offshore wind modeling
Sensitivity study
Atmosphere-wave coupling
WRF
Baltic Sea

ABSTRACT

Accurate wind modeling is important for wind resources assessment and wind power forecasting. To improve the WRF model configuration for the offshore wind modeling over the Baltic Sea, this study performed a sensitivity study of the WRF model to multiple model configurations, including domain setup, grid resolution, sea surface temperature, land surface data, and atmosphere-wave coupling. The simulated offshore wind was evaluated against LiDAR observations under different wind directions, atmospheric stabilities, and sea status. Generally, the simulated wind profiles matched observations, despite systematic underestimations. Strengthening the forcing from the reanalysis data through reducing the number of nested domains played the largest role in improving wind modeling. Atmosphere-wave coupling further improved the simulated wind, especially under the growing and mature sea conditions. Increasing the vertical resolution, and updating the sea surface temperature and the land surface information only had a slight impact, mainly visible during very stable conditions. Increasing the horizontal resolution also only had a slight impact, most visible during unstable conditions. Our study can help to improve the wind resources assessment and wind power forecasting over the Baltic Sea.

1. Introduction

With the fast development of wind power worldwide, there is a growing interest and dependence on the precise evaluation of wind resources and reliable prediction of wind power generation (Zheng et al., 2016; Murthy and Rahi, 2017; Veers et al., 2019). Numerical weather prediction (NWP) models can simulate the wind at a large scale and are powerful tools to wind energy studies. NWP models have been widely used for the production of wind atlases, forecasting of short-term wind power as well as prediction of future wind resources under future climate change scenarios (e.g. Greene et al., 2010; Olsen et al., 2017; Sanz Rodrigo et al., 2017). NWP models usually provide multiple options for model configuration and input data because of the various purposes of model applications. For accurate wind modeling, it is essential to evaluate the sensitivity of the model to these options.

Different model configurations for wind modeling, such as forcing data, domain setup, physical parameterization, land/sea surface information, have been widely evaluated (e.g. Santos-Alamillos et al., 2013; Hahmann et al., 2015, 2020; Floors et al., 2018a). The wind modeling accuracy has benefited from these sensitivity studies. However, most previous studies mainly focused on onshore wind, due to the early development of onshore wind farms and abundant observation data over the land (Zhou et al., 2020). Offshore wind energy has larger potential, as the wind over the sea is generally much stronger than over the land. To meet the urgent need for offshore wind energy exploitation, the sensitivity study of offshore wind modeling becomes very essential. Nevertheless, the sensitivity study of offshore wind modeling is still lacking in many areas, due to the few observation sites in the coastal zone and limited temporal extent of observation data (Zheng et al., 2016; Kalverla et al., 2019). This leads to the relatively poor understanding of the offshore wind field and the uncertainties of current offshore wind modeling (e.g. Karagali et al., 2018; Hallgren et al., 2020; Kalverla et al., 2020). For example, Kalverla et al. (2020) found that the New European Wind Atlas (NEWA) failed to improve upon ERA5 reanalysis data over the North Sea and even increased the random errors, despite an improvement over the land.

* Corresponding author.
E-mail address: huidong.li@geo.uu.se (H. Li).

https://doi.org/10.1016/j.gsf.2021.101229

Accurate offshore wind modeling is challenging in multiple aspects. The offshore wind field is largely affected by the land-sea interactions (Floors et al., 2013; Svensson et al., 2019a). In other words, the wind over the land could affect the offshore wind for quite a distance downstream from the coast (Hahmann et al., 2015). Therefore, the modeling of offshore wind also needs to consider the wind modeling over the upwind land (Floors et al., 2018a). Moreover, the air advection from the land to the sea can produce an internal boundary layer and low-level jets (LLJs), complicating the offshore wind modeling (Floors et al., 2013; Nunalee and Basu, 2014; Svensson et al., 2019a, 2019b; Hallgren et al., 2020). A dynamic ocean is another important influencing factor of the offshore wind field, due to the atmosphere–wave–ocean interactions, further increasing the difficulties in the accurate modeling of offshore wind (Kalvig et al., 2014; Wu et al., 2017). Sproson and Sahlée (2014) found that the simulated wind speed over the Baltic Sea with strong coastal upwelling could be reduced up to 3.5% in summer. Wu et al. (2016) recommended that the influence of swell on atmospheric mixing and wind stress should be considered in NWP models. However, most of the current offshore wind modelings do not couple the NWP models with wave models. Although the wave coupling was found to significantly affect long-term climate simulations, due to the accumulated influence and extreme weather events (Wu et al., 2016, 2017; Larsén et al., 2019), its impact on short-term and normal weather simulations is still unclear. Additionally, the initial and boundary conditions and domain setup also have impacts on the offshore wind modeling (e.g. Giannakopoulou and Nhili, 2014; Floors et al., 2018a; Hahmann et al., 2020).

Wind climatology varies largely with study areas and thus sensitivity study for a suitable model configuration is needed for any specific region. The Baltic Sea has abundant wind resources and is a hotspot for wind energy development (SWEA (Swedish Wind Energy Association), 2019). Since it is a high-latitude inland sea, the meteorological conditions of the Baltic Sea differ from the open sea. For example, the wind and turbulence fields over the Baltic Sea are highly influenced by the proximity to the coast (Svensson et al., 2019a). The Baltic Sea has distinct and frequent LLJs, which often occur at the height close to the turbine hub and therefore largely increase the wind energy (Hallgren et al., 2020). The offshore wind over the Baltic Sea is also sensitive to the atmosphere–wave–ocean interaction processes (Wu et al., 2020). Therefore, it can be expected that the sensitivity of the wind modelings to model setup over the Baltic Sea is different from other regions. However, the offshore wind modeling over the Baltic Sea is still rarely studied.

The Weather Research and Forecasting (WRF) model is one of the most popular NWP models for mesoscale wind energy studies. Both the NEWA and Global Wind Atlas were produced using the WRF model (Badger and Jørgensen, 2011; Hahmann et al., 2020). The WRF model is a state-of-the-art meteorological non-hydrostatic mesoscale model and has both research and practical versions. It is open-source and flexible, enabling users to change initial and boundary conditions, physical parameterization schemes, as well as grid resolution and nest domains, conveniently. The WRF model has been widely used for sensitivity studies of wind modeling under different physical parameterization options, initial and boundary conditions, grid nudging, integration time, etc. (e.g. Carvalho et al., 2012; Santos-Alamillos et al., 2013; Gomez et al., 2015; Hahmann et al., 2015, 2020). In the Baltic Sea region, Svensson et al. (2016, 2019b) preliminarily evaluated the WRF model in simulating offshore wind and the sensitivity to six boundary layer schemes and found that the WRF model underestimated the wind speed at turbine hub height and all boundary layer schemes had problems in capturing the strength and height of LLJs. Hallgren et al. (2020) found the NEWA data underestimated the average wind speed and shear over the Baltic Sea. The WRF model configuration for offshore wind modeling over the Baltic Sea still needs continuous improvement.

For a recommendation of what the WRF model configuration to use for offshore wind modeling over the Baltic Sea, we evaluated the sensitivity of the WRF model to multiple model setups, including the setup of domains and vertical levels, land surface data, and sea surface temperature data. Moreover, we studied the impact of wave coupling on the short-term wind simulation using an atmosphere-wave coupled model. Ten simulation experiments were designed in a chain to examine the sensitivity of these potential influencing factors one at a time. The simulated winds at both turbine hub height and wind profile were evaluated using LiDAR (Light Detection And Ranging) observations under different wind directions, atmospheric stabilities, and sea status. Our study can help to improve the assessment of wind resources and the forecasting of wind power over the Baltic Sea. Hopefully, the general conclusions that we draw about the model setup for the Baltic Sea are also valid for other large inland seas, thus facilitating and helping to improve future offshore wind modeling also elsewhere. The remainder of this paper describes the model setup, the design of simulation experiments, and evaluation method (Section 2), the model performance and its sensitivity to different setups (Section 3), and the conclusions and perspectives (Section 4).

2. Methodology

2.1. Model setup

2.1.1. Domain setup and physical scheme configuration

The WRF model version 3.8.1 was used. Three nested domains with a horizontal grid spacing of 9 km (D1), 3 km (D2), and 1 km (D3) were designed, with 190 × 178, 199 × 235, and 193 × 259 grid points, respectively (Fig. 1). The domain center was located at the island of Gotland, the largest island in the Baltic Sea. In the vertical direction, we applied two terrain-following Eta level division schemes, with 48 and 55 levels, respectively. The difference between these two schemes was located below 180 m, where the former set up 14 levels, while the latter set up 21 levels. The vertical resolution near the surface is very fine and then decreases gradually above. Referring to the previous study by Svensson et al. (2019b) in this region, we applied the following physical parameterization schemes: (1) the Dudhia (Dudhia, 1989) and the RRTM (Mlawer et al., 1997) schemes for shortwave and long-wave radiation, respectively; (2) the Thompson scheme (Thompson et al., 2008) for microphysics; (3) the Grell 3D scheme (Grell and Dévényi, 2002) for cumulus physics in domain 1; (4) the MYNN 2.5 scheme for the planetary boundary layer and the MYNN scheme for the surface layer (Nakanishi and Niino, 2009); and (5) the Noah LSM scheme (Tewari et al., 2004) for the land surface processes.

2.1.2. Atmosphere-wave coupling

To capture the dynamic feedback of the wave field on the atmospheric boundary layer, we implemented the UU-CM model (Uppsala University-Coupled model), which is a fully coupled atmosphere-wave-ocean-ice model (Wu et al., 2019). The UU-CM model estimates the stress on the air-sea interface as a balance of the air-side stress, ocean-side stress, wave-supported stress, and the momentum flux from waves to currents. In this study, only the atmosphere (WRF) and wave components (WaveWatch-III, WW3) are switched on. The WW3 model is a third-generation spectral wave model based on the wave energy balance equation. The WW3 model has been evaluated and successfully applied in the Baltic Sea before (Wu et al., 2016, 2020). The WRF model was coupled with the WW3 model through the OASIS3-MCT coupler

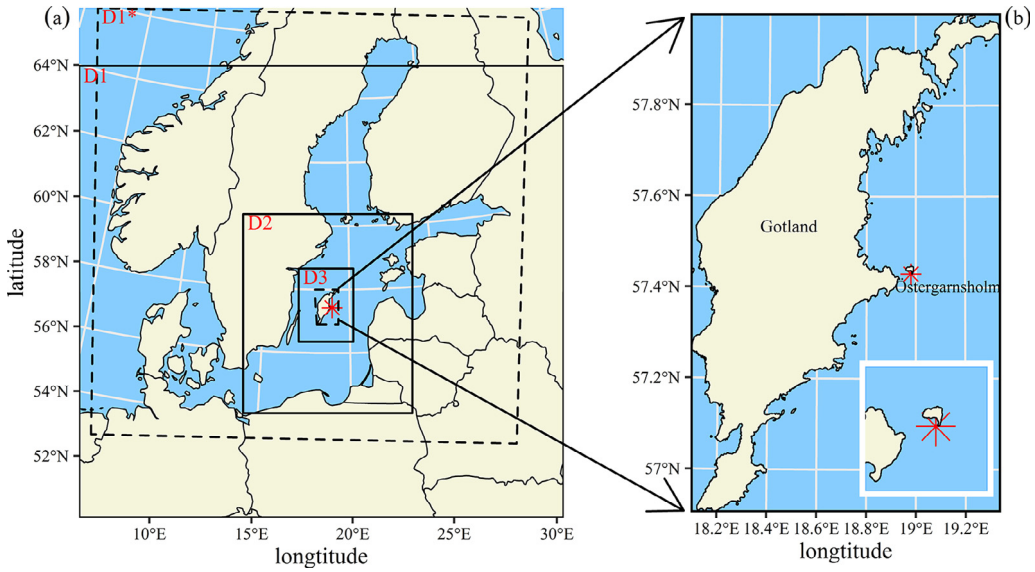

Fig. 1. (a) Domain setup and (b) the location of the observation site at Östergarnsholm.

(Valcke et al., 2013). In the stand-alone WRF model, the Charnock coefficient, used for estimating the surface roughness length, is estimated as a function of the mean wind speed. Accordingly, the Charnock coefficient is a constant for a given wind speed. However, the Charnock coefficient can be significantly affected by the wave state. Under a given wind speed, the Charnock coefficient is much larger under young waves than under old waves since waves extract more momentum from the atmosphere for wave growth. To capture the wave dynamical influences on the wind stress, in the UU-CM, the WRF model provides the wind field to WW3 for capturing the wave state. As feedback, WW3 provides the Charnock coefficient, estimated based on the 2D wave spectrum (Janssen, 1989), to the WRF model. In this way, the WRF model can capture the impact of the wave state on wind stress. The model components exchange variables every 10 min.

2.1.3. Initial and lateral boundary conditions

ERA5 reanalysis data at 37 pressure levels (the lowest layers are for every 25 hPa) were used as the initial and lateral boundary conditions. ERA5 data is a new generation reanalysis data from the European Centre for Medium-Range Weather Forecasts (ECMWF) with a spatial resolution of 0.28125° (~17 km × 31 km over the Baltic Sea) and 137 terrain-following hybrid sigma vertical levels (Hersbach et al., 2020). Variables are available on hourly analysis fields, which were generated through the 4D-var data assimilation used in ECMWF's Integrated Forecasting System cycle 41R2 with 12 h assimilation windows.

ERA5 data includes a sea surface temperature (SST) field. The ERA5 SST is interpolated from the daily OSTIA (Operational Sea Surface Temperature and Sea Ice Analysis) data with a resolution of 0.05°, which is derived from a combination of satellite and in-situ measurements since 2007 (Donlon et al., 2012). There are significant biases (underestimation in May but overestimation in November) of the coarse-resolution ERA5 SST in the study areas (Fig. 2). Given the influence of SST on offshore wind field simulations (Carvalho et al., 2012; Sproson and Sahlée, 2014), we also used DMI (Danish Meteorological Institute) SST product with a resolution of 0.02° as the lower boundary condition (Høyer and She, 2007). The DMI SST is based on satellite infrared and microwave radiometers from multiple sensors and provides daily gap-free maps of sea surface temperature for the Baltic Sea. Compared to the observations, although the DMI SST data also showed underestimation in May and overestimation in November, it was closer to the observed values than ERA5 data in both months (Fig. 2).

2.1.4. Land cover and topography datasets

Given the influence of land-sea interactions on offshore wind, the modeling of offshore wind also needs to consider the improvement of representations onshore. Topography and land surface information, such as roughness, are the key parameters of onshore wind modeling (Carvalho et al., 2012; Floors et al., 2013, 2018a). The WRF model applies a lookup table to determine the land surface parameters in each grid cell based on the dominant land cover type in the grid cell. The land cover data, therefore also becomes important input data of the WRF. The default topography and land cover data provided by the WRF model are USGS (United States Geological Survey) and MODIS (Moderate Resolution Imaging Spectroradiometer) data in 2001 with the highest resolution of 30 s. These data do not include the last two decades' change of land surface. Meanwhile, the land surface parameters in the lookup table represent the global mean conditions and cannot reflect the real conditions for a specific region. All of these problems may result in simulation errors.

We updated the topography using the Geographical Sweden Data (GSD) elevation product (Lantmäteriet, 2020) and the land cover data using Corine Land Cover (CLC) data (Feranec et al., 2010). The GSD data is produced by Lantmäteriet the Swedish mapping, cadastral, and land registration authority using laser scanning and has a resolution of 50 m. The CLC data is produced based on the photo-interpretation of satellite images by the national teams of the European Environment Agency member. The CLC data applies a 44-classification system and has a resolution of 100 m, enabling a better description of the real land cover. The CLC data has been widely used to drive the WRF model in Europe (Pineda et al., 2004; Li et al., 2018, 2020). More information about the CLC data can be found at https://land.copernicus.eu. In this study, the CLC data version 2018 was applied. To compare with default MODIS data and drive WRF model, we reclassified the CLC data to MODIS classification system with 21 land cover categories (Supplementary Data, Table S1), referring to the study by Pineda et al. (2004). Fig. 3 shows a comparison of default and updated topography and land cover maps. The elevation in GSD is often lower than the USGS database and captures more variation, even after interpolated to the same grid. Since the GSD data only covers

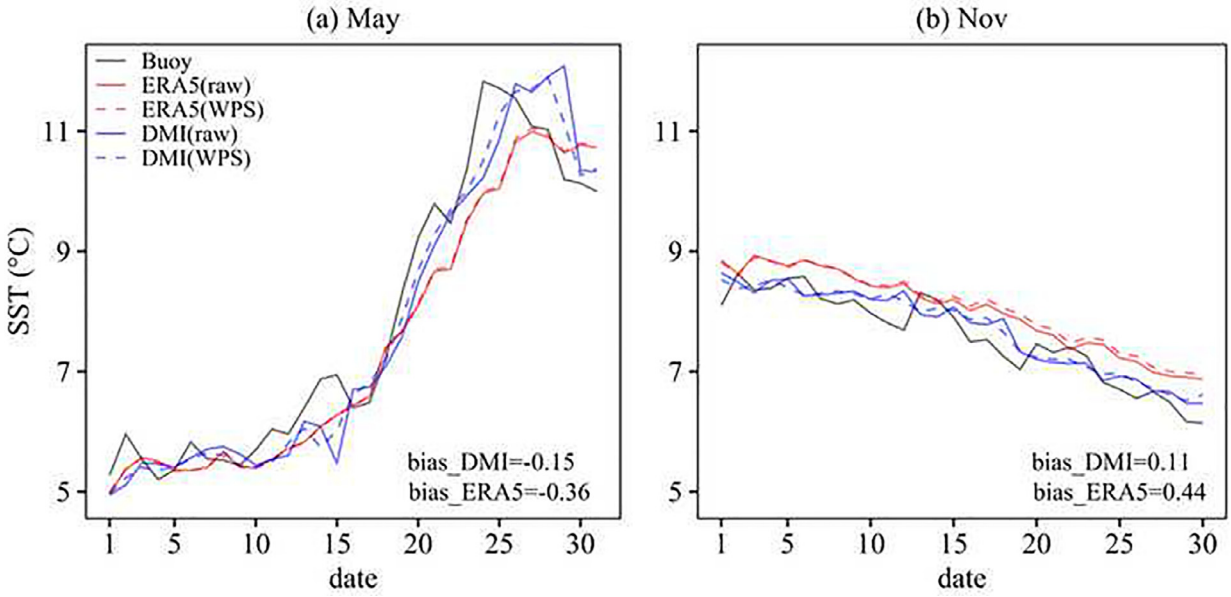

Fig. 2. Comparison of daily average SST from ERA5 and DMI datasets with buoy observations at the Östergarnsholm site in (a) May and (b) November 2017. The ERA5 and DMI SST were extracted from the nearest grid point to the observation site. Both the raw and interpolated data from WPS (WRF Pre-Processing System) are shown. The biases are calculated based on raw SST data.

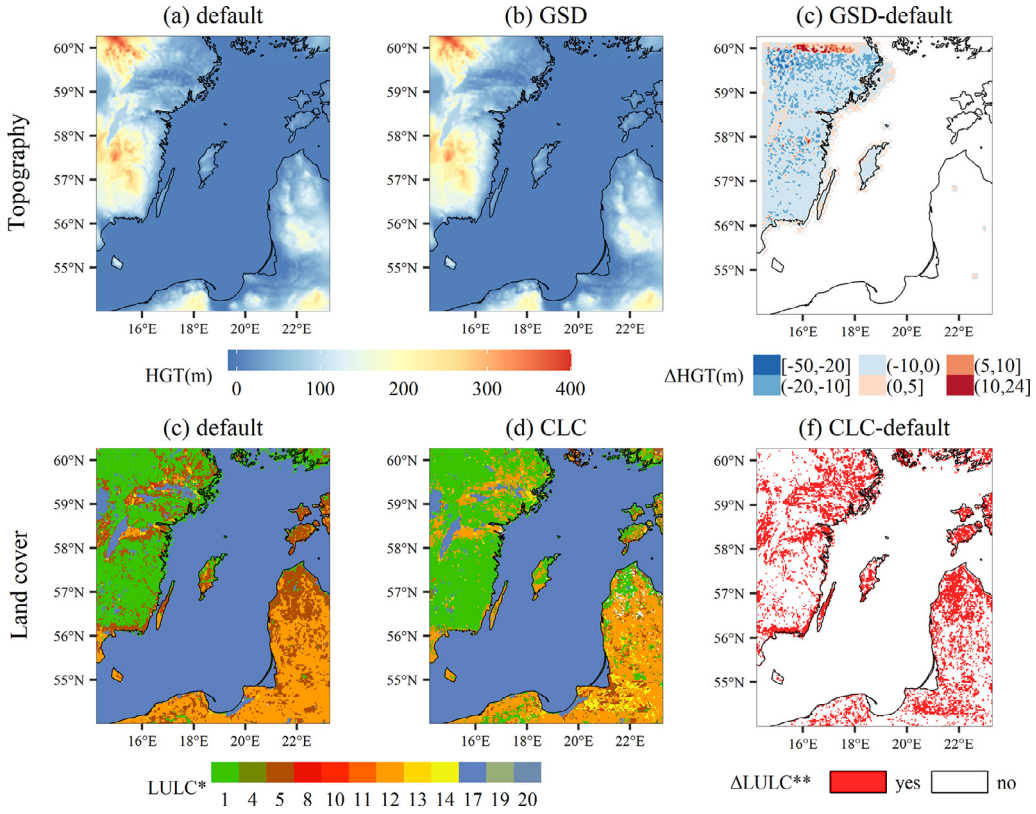

Fig. 3. Topography and land cover maps in domain 2. (a, b) show the default and updated CLC land cover data, and (c) shows their difference. (d, e) show the default and updated GSD topography data, and (f) shows their difference. *The numbering of the Land Use/Land Cover (LULC) types refers to Supplementary Data (Table S1). ** yes/no means whether the land cover category is different between default and CLC data or not.

Sweden, USGS topography was used outside Sweden. The major difference between the two land cover data is that larger areas in CLC are classified as agricultural or open land areas (category 12), but are classified as mixed forest (category 5) in MODIS data. In addition, we updated the lookup table by reducing the tree height to 65% and roughness to 80% of the default values of "Ever-

green Needleleaf Forest" and "Deciduous Broadleaf Forest" based on laser-scanned tree heights on the island of Gotland from the Swedish Forest Agency (https://kartor.skogsstyrelsen.se/kartor).

2.2. Simulation experiments

2.2.1. Simulation periods

We conducted simulations for two months in 2017: May when the marine atmospheric boundary layer stratification typically is stable and LLJs are common, and November when convection is more common over the sea (unstable stratification). For more details regarding the meteorological conditions during the two months, we refer to Section 3.1. The simulations were started every day at 12 UTC and lasted 36 h. The first 12 h of each simulation were taken as spin-up time and not included in the following analysis. The time-step was set as three times (in seconds) of the grid horizontal resolution (in km). For the atmosphere-wave coupled simulations, the coupling was switched on after the spin-up period. The WW3 was spin-up for 5 days before the first day run in each month.

2.2.2. Experimental design

Ten simulation experiments were set up in a chain to investigate the sensitivity of simulated offshore wind to domain setup, vertical layering, SST, land surface information, and atmosphere-wave coupling (Table 1). Run 1 is a reference case with almost the same settings as the study by Svensson et al. (2019b) in this region, except for the reanalysis data, ERA5 instead of ERA-Interim. It applied default static data and ERA5 SST data. Two domains, domain 1 and domain 2, were applied, with 48 vertical levels. The model output from domain 2 was used for the model evaluation. For run 2–6, we changed one influencing factor one-step at a time. Here we mainly describe the change at each step, compared to the previous ones. In run 2, we increased the vertical resolution to 55 levels. In run 3, we updated the input SST field using DMI data. In run 4, we updated the input static data using CLC and GSD data. In run 5, we updated the vegetation parameters with a decreased tree height and roughness and applied three domains. In run 6, domain 1 was not used, and then the simulation in domain 2 was forced by ERA5 directly. In both runs 5 and 6, we added domain 3 to investigate the impact of increasing horizontal resolution. The model outputs from domain 2 and 3 in the two runs were used to do the model evaluation represented by runs 5a and 5b, and 6a and 6b, respectively. As run 6 applied the default land use table, we compared run 6a to run 4 to investigate the impact of forcing data. In runs 7 and 8, the model was also forced by ERA5 directly, but we applied a larger domain (marked as D1* in Fig. 1) than that in run 6, with 500 × 500 grid points at a resolution of 3 km. The extent of the D1* was not the same as the other three domains, as they were jointly integrated into another project for studying the momentum conversion at the air-wave-sea interface (Qiao et al., 2021), but the options of physical schemes and the setup of vertical levels in runs 7–8 were the same as in runs 2–6. Due to technical reasons for the atmosphere-wave coupled simulation, these two runs only applied one domain. In run 8, we coupled the WRF model with the WW3. Given the different domain setups, we mainly compared the simulations of run 7 and 8 to reveal the impact of wave coupling and did not compare with other runs.

2.3. Model evaluation

2.3.1. Observation data

The observations were conducted at Östergarnsholm station (57°25′48.4″N, 18°59′2.9″E), located at the southern tip of a small island that is flat and has no trees at the central Baltic Sea just east of the island of Gotland (see Fig. 1). This site has been operating since 1995 and used in many air-sea interaction studies (e.g. Rutgersson et al., 2020). For wind profile measurements, a 30 m high tower is located at the site with instrumentation for wind speed and wind direction (Young Wind Monitor propeller anemometers) and temperature (ventilated and radiation shielded thermocouples, Type-T) at five heights 7, 11.5, 14, 20, 28 m above the tower base. Additionally, the tower is instrumented with a sonic anemometer (CSAT-3D) for turbulence measurements at 9 m. Sea level variations at the site are quite small and the tower base is located 1 ± 0.5 m above mean sea level. For a more detailed description of the instrumentation, we refer to the site evaluation made in Rutgersson et al. (2020). For measurements of the wind profile above 28 m, we used a conically scanning, continuous-wave LiDAR (ZephIR 300 ZX Lidars, UK) placed approximately 40 m north of the tower. The LiDAR measurement heights were set to heights 28, 39, 50, 100, 150, 200, 250, and 300 m above sea level (Svensson et al., 2019b; Hallgren et al., 2020). Wave measurements including directional properties were conducted from a moored Directional Waverider 4 km southeast of the island of Östergarnsholm, operated by the Finnish Meteorological Institute. The mooring was placed at a location with 39 m depth, and also measured the water temperature at 0.5 m depth. All observations were averaged over 30 min periods.

2.3.2. Data processing and evaluation metrics

To obtain the simulated wind at a specific height, we conducted vertical interpolation of the raw simulated wind from the Eta levels to height levels (0–1000 m above the sea level) using the WRF-Python package (https://wrf-python.readthedocs.io/en/latest/). Below 300 m, the height of interpolation levels was set to be the

Table 1
Setup of simulation experiments.

Run ID		Domain ID	Boundary condition	Horizontal resolution	Vertical levels	Static data	SST data	Wave coupling	Land use table
1		2	D1 output	3 km	48	default	ERA5	No	default
2		–*	–	–	55	–	–	–	–
3		–	–	–	–	–	DMI	–	–
4		–	–	–	–	GSD + CLC	–	–	–
5	a	–	–	–	–	–	–	–	↓H&f**
	b	3	D2 output	1 km	–	–	–	–	–
6	a	2	ERA5	3 km	–	–	–	–	default
	b	3	D2 output	1 km	–	–	–	–	–
7		1***	ERA5	3 km	–	default	–	–	–
8		–	–	–	–	–	–	Yes	–

* dash means that the item is the same as in the former run.
** ↓: decrease; H: tree height; *f*: roughness.
*** domain 1 of runs 7–8 is not the same with other runs.

same as the tower and LiDAR observation heights. Steps of 50 m were used between 300 and 500 m, and 100 m from 500 to 1000 m. The data at the grid point nearest to the observation site was extracted for the model evaluation. We first compared the simulated wind profiles against the LiDAR observation and then used different indices, including correlation coefficient (r), mean bias (MB), and root mean square error (RMSE), to quantify the model performance at 100 m. We chose 100 m following the study by Svensson et al. (2019b), as it is close to the typical hub height of offshore wind turbines and can reflect the influence of mesoscale effects. Besides, we applied Taylor diagrams to show the performance at four levels around hub height (50, 100, 150, and 200 m).

2.3.3. Evaluation under different meteorological and sea state conditions

We evaluated the model performance under several conditions, including different wind directions, atmospheric stabilities, and wave ages (Table 2). Offshore winds in coastal areas are affected by the airflow from both the land and sea. Rutgersson et al. (2020) classified the wind from different directions to represent different upstream types of surface influence at the Östergarnsholm site. Accordingly, we divided the wind direction into three sectors: the Sea, Gotland, and Östergarnsholm sectors. The wind from the sea sector represented the influence of the open sea, while the wind from the Gotland sector represented the influence of the land. The wind from the Östergarnsholm sector was influenced by the island of Östergarnsholm (Fig. 1), however, the simulations cannot resolve this island as the size of the island is too small for the horizontal resolution. Atmospheric stability is another important influencing factor of wind modeling. Svensson et al. (2019a,b) found that the WRF performance in simulating offshore wind varied largely with atmospheric stability conditions in the study region. Accordingly, we divided the study period into five atmospheric stability categories: very unstable (VU), moderate unstable (MU), neutral (N), moderate stable (MS), and very stable (VS) based on the dimensionless height $z\ L^{-1}$, where z is height and L is the Monin-Obukhov length (Svensson et al., 2019a). The Monin-Obukhov length was calculated using the flux measurements in the tower at 10 m above sea level as $L = -u_*^3\ \bar{\theta}_v\ /kg\overline{w'\theta'_v}$, where u_* is the frictional velocity (m s^{-1}); g is the acceleration of gravity (9.8 m s^{-2}); k is the von Karman constant (0.4); is the virtual air temperature (K); is the surface virtual potential temperature flux (K m s^{-1}).

Ocean waves directly interact with the atmosphere by changing the roughness of the sea surface. Growing waves extract momentum from the airflow and slow down the wind. In contrast, swell waves interact with the atmosphere, forcing the atmosphere from below, and even positive momentum fluxes have been observed during such conditions (e.g. Högström et al., 2015, 2018; Wu et al., 2016). Based on the wave age, we divided the study period into three categories: growing sea, mature, and swell. The wave age was defined as U/C_p, where U is the wind speed at 8 m above the sea and C_p is the phase speed of waves at the peak of the wave spectrum. The phase speed was calculated based on the solution of the dispersion equation and the observed peak frequency by the wave buoy.

3. Results and discussions

3.1. Meteorological conditions during the study period

A summary of the meteorological conditions measured at the Östergarnsholm station is shown in Fig. 4. In May, the air temperature was higher than the SST, leading to the stable atmospheric stratification, and vice versa during November with the unstable atmospheric stratification. The wind was stronger in November than May, with the speed at 100 m of 8.95 ± 3.56 (mean ± standard deviation) and 7.52 ± 3.79 m s^{-1}, respectively. The wind directions were generally opposite between these two months. In May, most of the winds were directed from the open sea or the small island of Östergarnsholm, while in November, most of the winds were directed from the island of Gotland. During most of the time, the wave field was in swell conditions. In general, the wave age is inversely proportional to the wind speed and in November, the wave age indicated more growing sea and mature conditions compared to May.

3.2. Overall model performance and sensitivity

3.2.1. Wind profiles

Generally, all the simulations underestimated wind speed in the average profiles (Fig. 5). The systematic underestimation of WRF simulated offshore wind is likely to inherit from ERA5, as discussed in the study by Hallgren et al. (2020) and Kalverla et al. (2020), who found that both the ERA5 and NEWA underestimated the mean wind speed profile over the Baltic and North Sea, respectively. More details about the evaluation of ERA5 data at the observation site were described in Section 3.2.2. In May, the observed wind showed on average a weak LLJ with a core at around 200 m (Fig. 5a). However, all the simulations underestimated the strength of the average LLJs. Runs 6–8 directly forced by reanalysis data reproduced the LLJs in the average profiles, but with the core at higher levels, compared to the observed. The mismatch of the core height of LLJs between simulations and observations was also found in many previous studies (e.g. Floors et al., 2013; Svensson et al., 2019b; Kalverla et al., 2020). The average LLJs in runs 1–5 with domain 1 were rather minor. The observations in November showed stronger winds and wind shear, but no LLJs in the average wind profile. The underestimation of wind simulation in November increased with the height, leading to the underestimation of wind speed shear, consistent with the analysis of the NEWA data (Hallgren et al., 2020; Kalverla et al., 2020).

Among all the simulations, the average wind profiles in run 6 directly forced by reanalysis data were closest to the observed, especially in November. The better performance of run 6 than other runs indicates that using ERA5 as the boundary conditions

Table 2
Division of simulation period based on the wind direction, atmospheric stability, and wave age.

Wind direction		Atmospheric stability		Wave age	
Division	Degree	Division*	Value	Division	Value
Sea	(45, 220)	VU	$(-\infty, -0.2)$	Swell	$(1.2, +\infty)$
Gotland	(220, 295)	MU	$(-0.2, -0.05)$	Mature	(0.8,1.2)
Östergarnsholm	(295, 45)	N	$(-0.05, 0.05)$	Growing sea	(0,0.8)
		MS	(0.05, 0.2)		
		VS	$(0.2, +\infty)$		

* VU: very unstable; MU: moderate unstable; N: neutral; MS: moderate stable; VS: very stable.

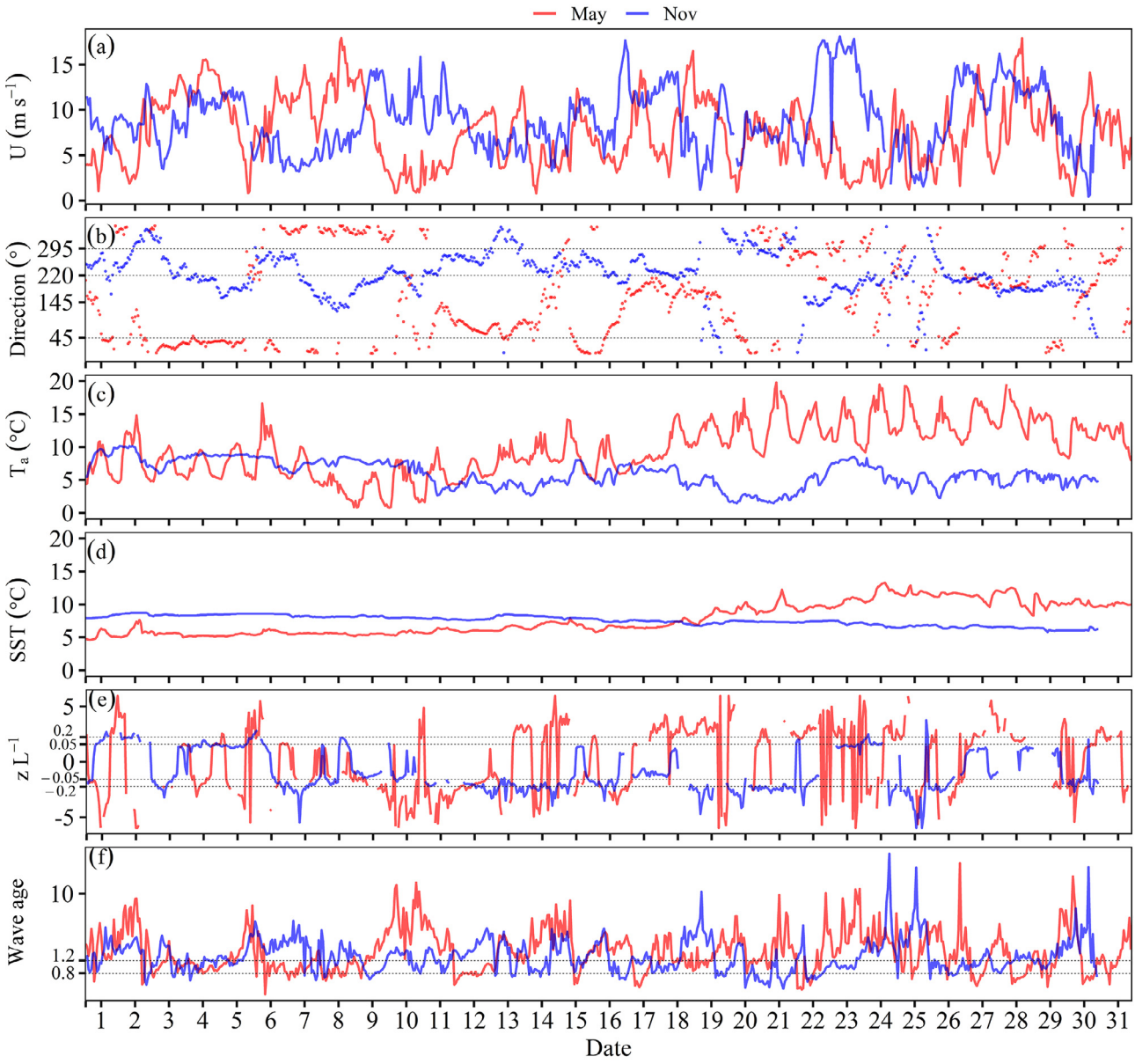

Fig. 4. Time series of observed (a) wind speed at 100 m, (b) wind direction at 8 m, (c) air temperature at 8 m, (d) SST, (e) $z\ L^{-1}$ (z = 10 m), and (f) wave age at the Östergarnsholm site during the study period. Values of $z\ L^{-1}$ greater (less) than 10 (−10) were plotted as 10 (−10). Note the scales of $z\ L^{-1}$ and wave age are cube root and logarithmic, respectively. The dashed lines represent the division of the simulation period as shown in Table 2.

directly in domain 2 is better than using the simulation results from domain 1. This is because the nested domains decreased the direct impact of reanalysis data on the simulations in domain 2 and even may introduce new bias in the simulation in domain 1. We discussed the large impact of direct forcing from reanalysis data in Section 3.2.2. The simulated average wind profiles of run 6a from domain 2 and 6b from domain 3 only showed small differences, mainly located at 300–500 m where the simulated LLJs appeared in May, and 50–500 m where distinct wind shear appeared in November, and the difference in November was slightly larger, compared to that in May. The comparison of run 5a and run 5b showed similar results. This indicates that adding a domain with finer resolution than 3 km failed to significantly improve offshore wind modeling, which is consistent with the conclusions of the studies by Carvalho et al. (2012) and Floors et al (2018b). Run 7 applied the same model setup as run 6, except for a larger domain. However, the simulated wind speed profile in run 7 was more biased than in run 6. The positive influence from the direct forcing of reanalysis data was likely partly offset by the larger domain in run 7, as the influence gradually decreased from the boundary to the domain center. Additionally, the impact of forcing data on the wind modeling caused by the domain setup varied with time and height. Generally, the decrease in the simulated biases of run 6, compared with other runs, was much larger in November and located higher up. Furthermore, these results were also valid for relative biases (Supplementary Data, Fig. S1), implying a larger sensitivity of simulated wind to forcing data in November and at higher levels. The simulated wind profiles of run 8 with atmosphere-wave coupling were closer to the observed, compared to run 7, implying a positive role of atmosphere-wave coupling in modeling offshore wind. The simulated wind profiles among runs 1–5 with the increased vertical resolution, updated SST and land surface information showed slight improvements in May, but minor differences in November. The more stable

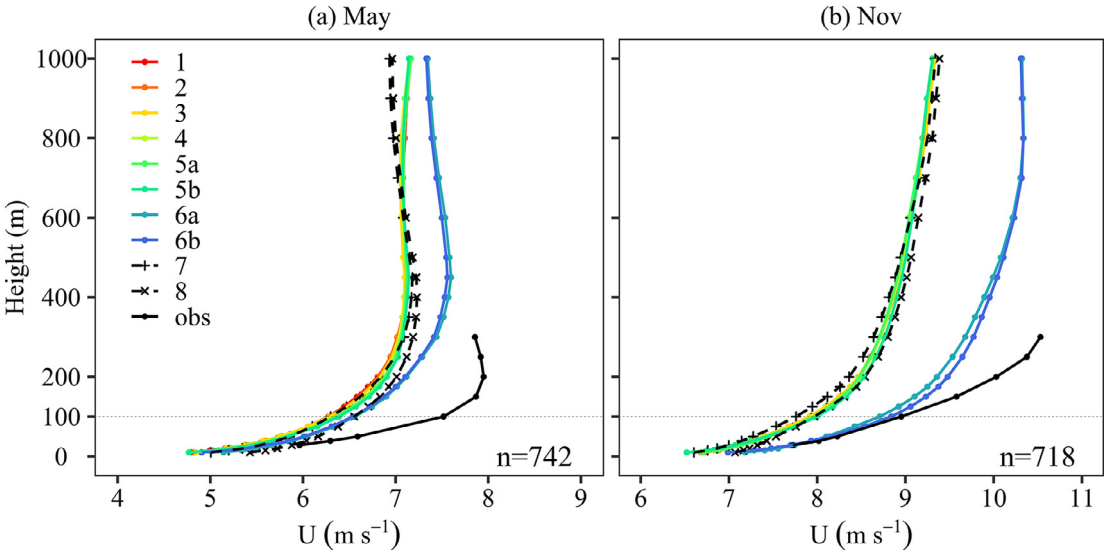

Fig. 5. Comparison of the simulated and observed average wind speed profiles at the Östergarnsholm site in (a) May and (b) November. n indicates the number of cases averaged in each profile.

boundary layer in May was likely to be the reason for the positive impact of improving land/sea surface information, which was further discussed in Section 3.3.2.

3.2.2. Wind at hub height

The difference in the simulated wind speed around turbine hub height (~100 m) among all the simulations is generally consistent with that in the simulated wind profiles. At 100 m height, run 6 directly forced by ERA5 data outperformed the runs 1–5 (Fig. 6), with the RMSE of 2.50 and 2.22 m s^{-1} for run 6a in May and November respectively, the MB of −0.95 and −0.23 m s^{-1}, and a correlation coefficient of 0.79 and 0.81 (Table 3). Furthermore, the standard deviation (STD) of run 6 was closer to the observed, especially in November, implying that run 6 also simulated the temporal variations of wind speed better than the other runs. Runs 7 and 8 were also directly forced by ERA5 data and showed high accuracy in simulating offshore wind at hub height. To explain the largest impact of direct forcing from the reanalysis data, we evaluated the ERA5 data at 100 m against the LiDAR observation (Fig. 6b, f, and Table 3). The ERA5 data shows higher accuracy than all the WRF simulations, with the RMSE of 1.82 and 1.71 m s^{-1} in May and November respectively, the MB of −0.78 and −0.52 m s^{-1}, and the correlation coefficient of 0.90 and 0.89. This result is consistent with a recent study by Kalverla et al. (2020), which also found increased random errors in the WRF-based NEWA data, compared to the ERA5 data, and attributed this to a substantial

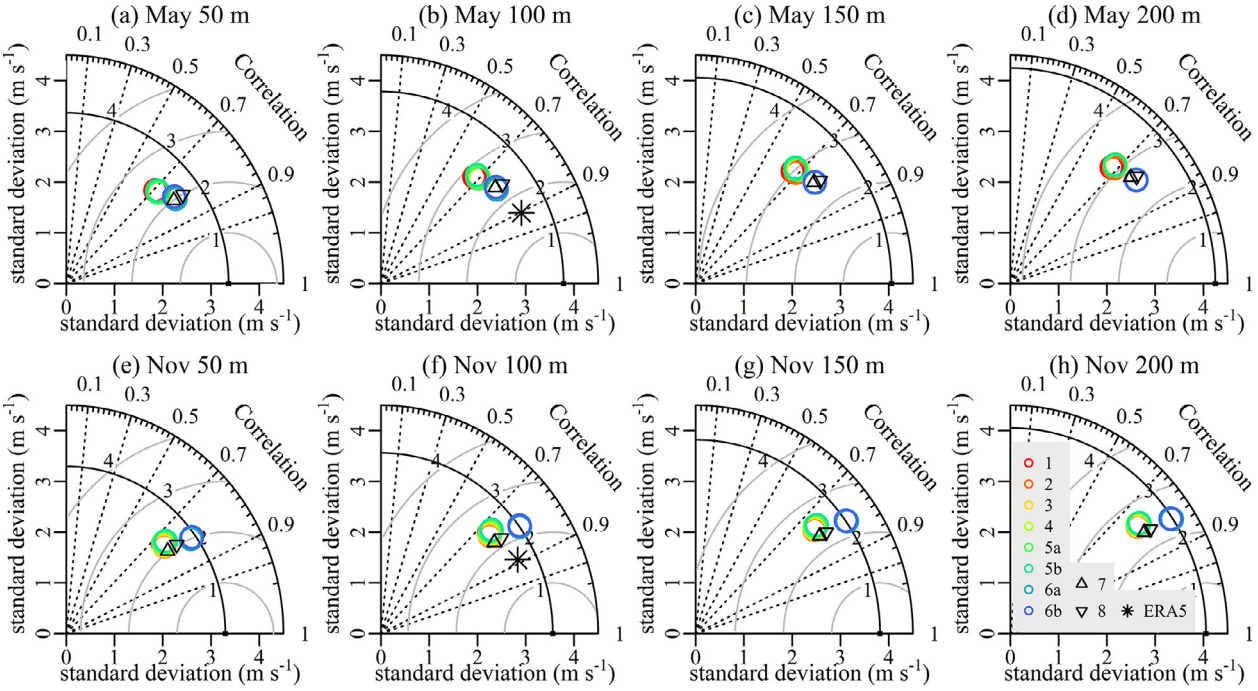

Fig. 6. Taylor diagram of wind speed at (a, e) 50, (b, f) 100, (c, g) 150, and (d, h) 200 m at the Östergarnsholm site. (a–d) show the results in May, and (e–h) show the results in November.

Table 3
Statistic of model performance in simulating wind speed at 100 m at the Östergarnsholm site compared to LiDAR observations.

Run ID	Correlation coefficient		Mean Bias (m s^{-1})		RMSE (m s^{-1})	
	May	Nov	May	Nov	May	Nov
1	0.68	0.75	−1.23	−1.01	3.06	2.59
2	0.69	0.76	−1.21	−1.02	3.00	2.54
3	0.69	0.76	−1.22	−1.03	3.02	2.56
4	0.70	0.75	−1.16	−0.97	2.94	2.57
5a	0.70	0.75	−1.15	−0.98	2.96	2.59
5b	0.68	0.75	−1.12	−0.94	3.00	2.58
6a	0.79	0.81	−0.95	−0.23	2.50	2.22
6b	0.78	0.80	−0.97	−0.10	2.55	2.24
7	0.78	0.79	−1.21	−1.18	2.66	2.47
8	0.79	0.80	−0.96	−0.97	2.52	2.37
ERA5	0.90	0.89	−0.78	−0.52	1.82	1.71

double penalty. Strengthening direct forcing from the ERA5 data can decrease the random errors and therefore improve the offshore wind modeling. Meanwhile, the ERA5 data also showed underestimation in both months. These results are consistent with the study by Hallgren et al. (2020) and explain the underestimation of the WRF simulations.

The simulated offshore wind at hub height from run 8 (with wave-coupling) showed higher accuracy than that from run 7 (without wave-coupling) implying a positive impact of atmosphere-wave coupling. The simulated wind speed at 100 m differed slightly among runs 1–5. Only in May, the model performance of runs 1–5 with the increased vertical resolution, updated SST and land surface information showed slightly gradual improvements in the chain of runs. The differences in the simulated wind speed at 100 m between runs 6a (5a) from domain 2 and 6b (5b) from domain 3 were also small. The run 6b only slightly decreased the simulated mean bias in November, compared to run 6a.

Generally, the model performed better in simulating hub-height wind in November with the smaller absolute biases, despite the stronger winds, compared to in May. Furthermore, the STD of simulations was much closer to that of observations in November, implying that the simulations could better reproduce the temporal variation of wind speed during this period. Due to the frequent LLJs, the observed hub-height winds in May showed larger temporal variations with a larger STD despite a smaller wind speed. The failure in simulating the LLJs is likely the major reason for the worse evaluation metrics of the May simulations.

3.3. Sensitivity of the simulated profiles under different conditions

3.3.1. Varying wind direction

The model performance varied with the wind direction sectors (Fig. 7). Here, the selection of data was conditioned such that both modeling and observational data had to fulfill the wind sector criteria defined in Table 2 at the same time. Comparing the different sectors, the simulated winds from the Gotland sector showed the least bias, while the simulated winds from the Sea and Östergarnsholm sectors showed significant underestimations. Among the different runs, run 6 with direct forcing produced higher wind speed, especially in November, leading to the significant improvement of the simulated wind from the Sea sector and the slightly overestimated wind speed from the Gotland sector. In May, the simulated wind from the Sea sector reproduced the LLJs, but with the core located too high up. The observed average wind profiles from the Gotland sector did not show LLJs, but the simulated wind included LLJs in the average profile. The poor representation of atmospheric stability by the boundary layer scheme is likely the reason for the mismatch between observations and simulations (Floors et al., 2013; Kalverla et al., 2020), which is further discussed in the next section. The comparison of observed and simulated winds from the Östergarnsholm sector indicates large uncertainties in the simulations, showing the largest biases in May and qualitatively different profiles in November, as the observed winds from this sector were affected by the small island, but the model ignored this impact due to the much smaller area of the island, compared to the grid size.

3.3.2. Varying atmospheric stability

The model performance showed some variations with atmospheric stabilities (Fig. 8). In May, all the simulations showed the largest biases under neutral conditions. The observations showed distinct LLJs under stable and neutral conditions. However, the simulations of runs 1–5 forced by the simulations in domain 1 only showed weak LLJs in the average profile during neutral and very stable conditions, and the simulations of run 6 forced directly by the ERA5 only showed LLJs during neutral and moderate stable conditions. The difference between run 6 and the other runs was not significant under very stable conditions. Although run 6 increased the simulated wind speed in magnitude under neutral conditions, the core height of the simulated LLJs in the average profile was located too high as for the other runs. These all indicates that the failure in capturing the LLJs was not closely related to the forcing data. The difference between observations and simulations in the LLJs is more likely caused by the poor representation of atmospheric stability by the boundary layer scheme, especially the stable conditions, which is the major reason for the LLJs over the Baltic Sea (Hallgren et al., 2020). Similar conclusions were also drawn by the previous studies in other areas (e.g. Floors et al., 2013; Holtslag et al., 2013). In addition, both the observations and simulations showed weak LLJs in the average profile under moderately unstable conditions. This may be caused by the disturbance of other factors, such as wind direction, which had a high degree of variation during the study period (Fig. 4). In November, the simulated wind profiles of most runs became closer to observations when the atmosphere changed from neutral to more stable/unstable, consistent with that in May. Run 6 directly forced by reanalysis data showed better performance than the other runs under most of the stability conditions. Furthermore, the difference between run 6 and other runs reached its maximum under neutral conditions, implying a larger impact of forcing data on the wind simulations for the neutral marine atmospheric boundary layer. In both months, the simulations of runs 1–5 with the increased vertical resolution, updated SST and land surface information showed larger differences under the very stable conditions, compared to other conditions, especially in May. This could be the reason for the difference in the simulated average wind speed profiles among runs 1–5 in May (Fig. 5), due to more cases with very stable stratification. In contrast, the simulations of runs 6a from domain 2 and 6b from domain 3 showed larger differences under the unstable conditions in November.

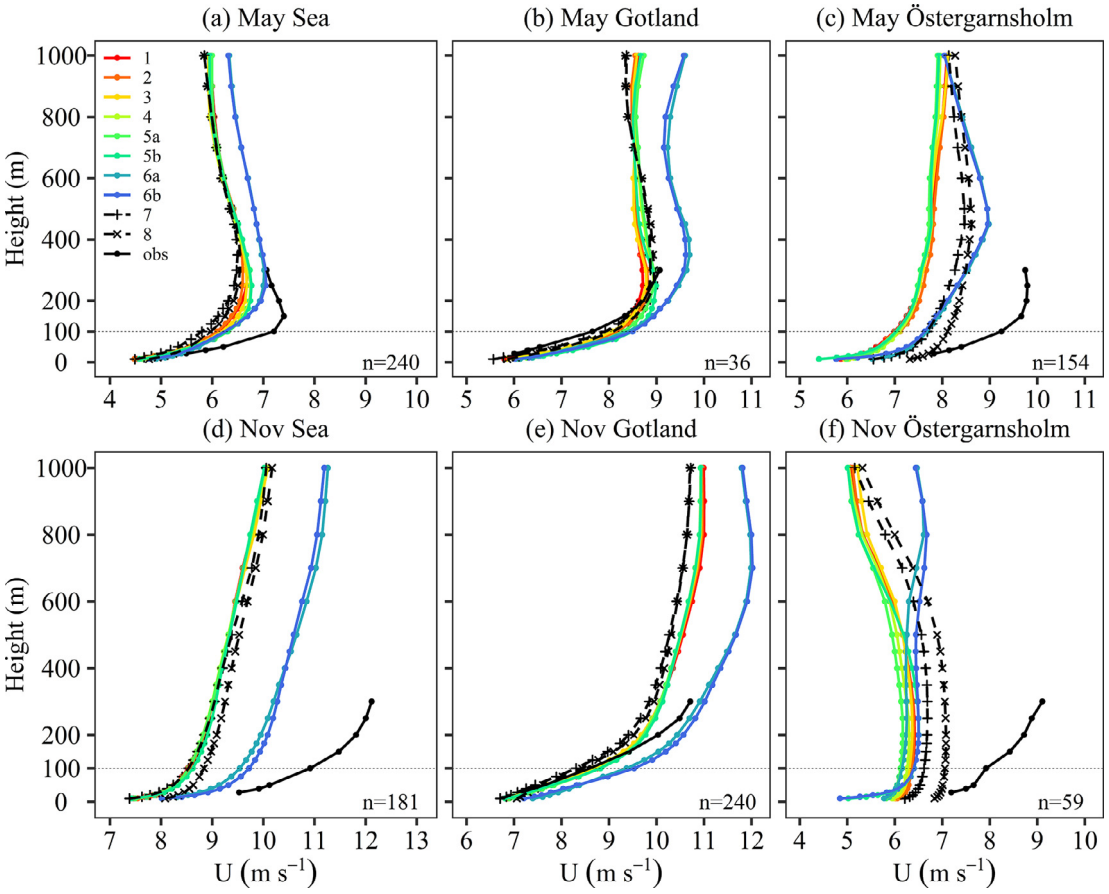

Fig. 7. Comparison of the simulated and observed average wind speed profiles from different wind direction sectors at the Östergarnsholm site. (a–c) show the results in May, and (d–f) show the results in November. Only time steps from the same direction sectors in both observations and simulations are included. The title above each subfigure marks the wind sectors defined in Table 2, and n indicates the number of cases averaged in each profile.

3.4. Sensitivity of the simulated wind field to different model setups

We further investigated the difference of the simulated offshore wind maps at 100 m among runs 1–6 one step at a time to examine the sensitivity of the simulated wind fields to different model setups. Generally, the difference between run 6, forced directly by the ERA5, and run 4, forced by the simulations in domain 1, was larger than others (Fig. 9e, j), implying the important role of direct forcing on the simulated offshore wind. The impact of forcing data in domain 2 transferred from the domain border to the domain center. The difference between runs 6 and 4 over the sea showed a mix of both positive and negative values in May (Fig. 9e), while it was mainly positive in November (Fig. 9j). The positive impact of forcing data could compensate for the underestimation of the simulated wind (Fig. 5 and Table 3), increasing the simulated accuracy. Especially in November, the difference between runs 6 and 4 was significant (Supplementary Data, Fig. S2e, k), implying a more important impact of the direct forcing, consistent with the results of model evaluation. Run 2 with 55 levels generally produced stronger offshore winds at 100 m (Fig. 9a, f), compared to run 1 with 48 levels, implying a positive impact of increasing vertical resolution. However, the impact of increasing the vertical resolution was not significant (Supplementary Data, Fig. S2a, g) and limited with an increase in the simulated wind speed in run 2 less than 0.1 m s^{-1}. Updating SST and land surface information also showed limited impacts on the simulated offshore wind at 100 m. The difference of the simulated wind between run 3 with the DMI SST and run 2 with the ERA5 SST was within ±0.2 m s^{-1} with both negative and positive values and without a dominant trend. The change of the simulated wind caused by updating GSD topography and CLC land cover in run 4 (Fig. 9c, h) and updating tree height and roughness in run 5 (Fig. 9d, i) was rather minor, within ±0.1 m s^{-1}. For increasing the vertical resolution and updating SST and land surface information, their impacts on the simulated offshore winds were larger in May than in November, which is likely related to the more frequently occurring stable conditions in this month (Fig. 8e).

3.5. Sensitivity to atmosphere-wave coupling

The model performance in modeling offshore wind varied with the wave age conditions. Fig. 10a shows the variation of the simulated wind speed bias of run 8 with atmosphere-wave coupling under different wave age conditions. The biases were negative when the wave age was very small and decreased with the increase in wave age until around 3 (young swell waves), then became positive and increased gradually after that. The simulations underestimated the wind speed for most cases in the growing sea, mature, and early swell conditions, but overestimated the wind speed for some cases in the late swell condition. Furthermore, the underestimation was more significant than the overestimation in May. Regarding the simulations at different levels, the underestimation under young wave age conditions was more significant at high levels, and the overestimation under large wave age conditions was more significant at low levels. Nevertheless, due to the opposite trend of wind speed and wave age (Fig. 4), the relative overestimation under the swell condition was larger than the underestimation under the growing sea condition (Supplementary

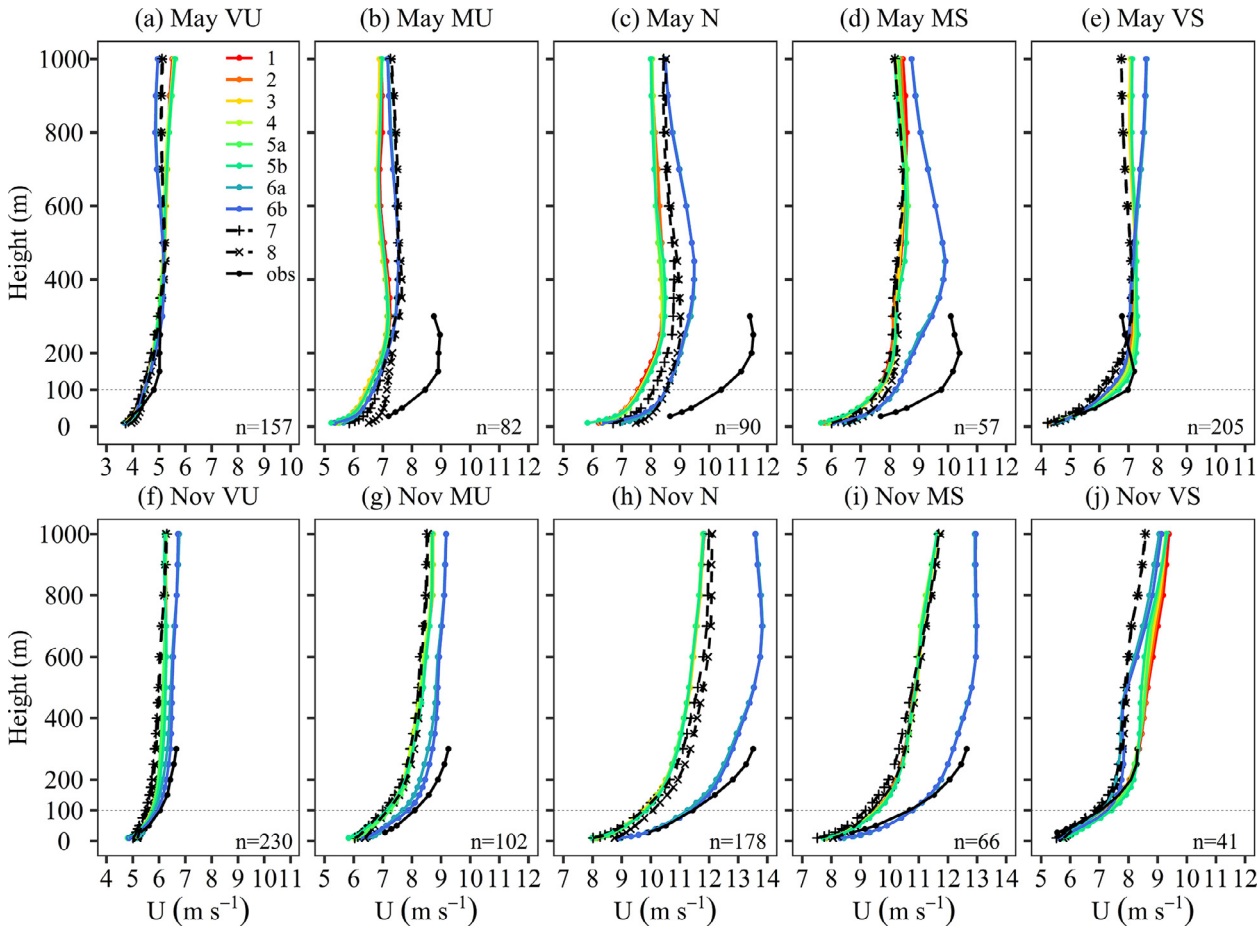

Fig. 8. Comparison of the simulated and observed average wind profiles under different atmospheric stability conditions at the Östergarnsholm site. (a–e) show the results in May, and (f–j) show the results in November. The title above each subfigure marks the stability regime defined in Table 2, and n indicates the number of cases averaged in each profile.

Data, Fig. S3a). Meanwhile, due to the stronger wind at high levels, most of the relative bias among different levels became minor.

The impact of atmosphere-wave coupling on the offshore wind modeling was also correlated with wave age conditions (Fig. 10b). In May, the difference of simulated wind speed between run 8 with wave coupling and run 7 without wave coupling increased with the increase in wave age first under growing sea condition, reached high values under mature condition, then decreased gradually with wave age under swell condition (Fig. 10b). In November, the overall difference decreased continuously with wave age. The relative difference of the two runs also decreased with wave age, but with a smaller decreasing trend in May (Supplementary Data, Fig. S3b). Both the absolute and relative differences decreased with height and became rather small at heights close to 1000 m. Moreover, the difference between different levels was more significant at growing sea and mature wave conditions (Supplementary Data, Fig. S3b). These indicate that the atmosphere-wave coupling played a more important role in improving the offshore wind modeling under growing sea and mature conditions than under swell conditions and that the role of atmosphere-wave coupling decreased with height.

Run 8, with wave coupling, increased the simulated offshore wind speed at 100 m, compared to run 7, without wave coupling, in the entire domain during both May and November (Fig. 11), implying the positive impact of atmosphere-wave coupling. Furthermore, the sensitivity of simulated wind to the atmosphere-wave coupling seems to be larger than most of the other model setups and is only surpassed by the altering forcing strategy in run 6. The increased simulated wind showed spatial and temporal variations. Generally, the increase in the simulated wind was larger over the open sea far from the coast compared to closer to the coastline, consistent with the study by Wu et al. (2020). The overall impact of atmosphere-wave coupling was larger and more significant in November than in May (Supplementary Data, Fig. S2f, l). The median value of the increased wind speed at 100 m in run 8 was 0.28 m s^{-1} in May and 0.41 m s^{-1} in November. However, due to the stronger winds in November, the difference in the relative increase in the wind speed between the two months was minor, with median values of 4.18% and 4.19%, respectively.

4. Conclusions and perspectives

To improve the WRF model configuration for the offshore wind modeling over the Baltic Sea, we performed a sensitivity study to multiple model setups under different wind directions, atmospheric stabilities, and sea status. Generally, the simulated wind profiles could capture the LiDAR observed but showed systematic underestimations. The model generally performed better under very stable/unstable conditions than under neutral conditions. The simulations forced directly by the ERA5 reanalysis data through reducing the number of nested domains significantly outperformed others, especially when the wind was from the sea sector and under neutral conditions. Atmosphere-wave coupling

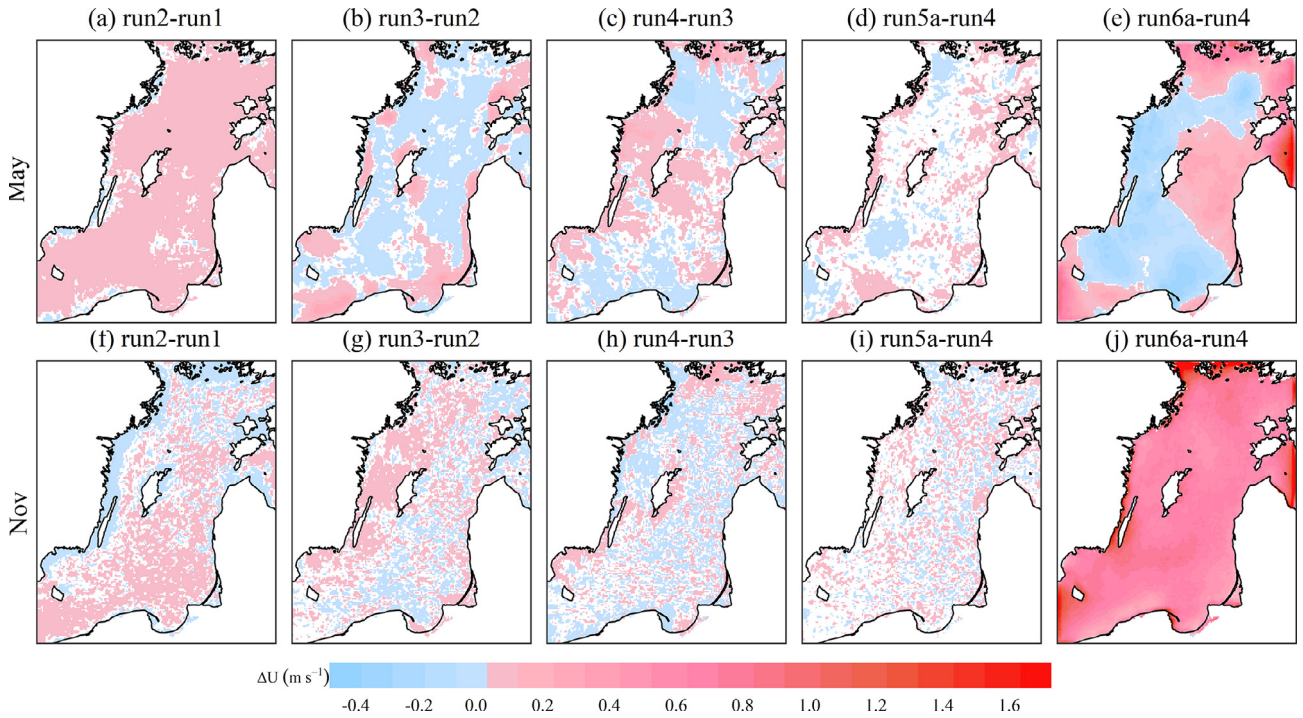

Fig. 9. Difference of the monthly mean simulated offshore wind fields at 100 m among run 1 to 6 in (a–e) May and (f–j) November. Difference less than ±0.01 m s^{-1} is shown in white. The five columns from left to right reflect the impact of (a, f) increasing vertical layers, (b, g) updating SST, (c, h) updating land surface information, (d, i) updating forest parameters, and (e, j) direct forcing from ERA5 data.

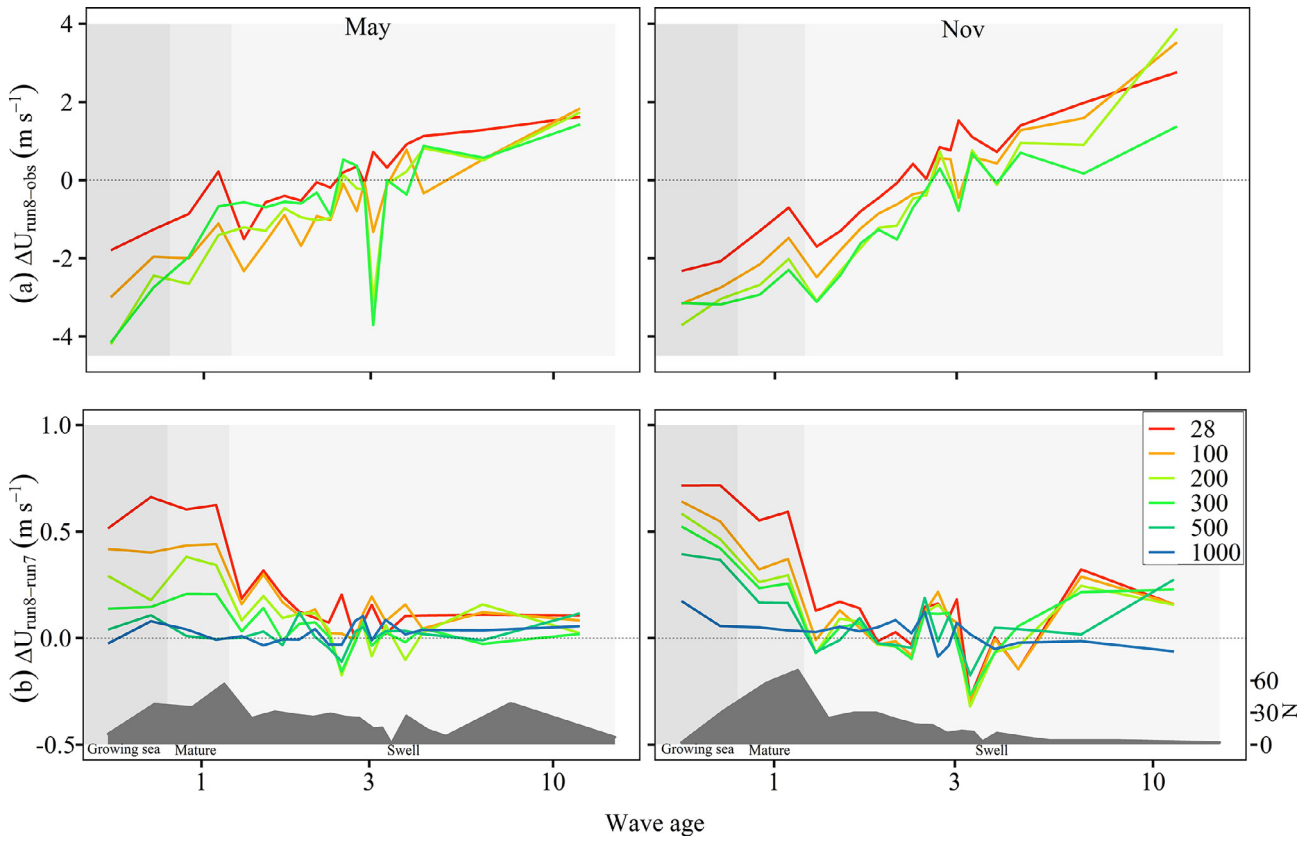

Fig. 10. The variations of (a) the simulated offshore wind speed biases of run 8 (with wave coupling) compared to LiDAR observations and (b) the difference in the simulated wind speed between run 7 (without wave coupling) and 8 with the change of wave age at the Östergarnsholm site in (left) May and (right) November. Only time steps under the same wave conditions (growing sea, mature, swell) in both observations and simulations are included. Annotations above the *x*-axis mark the wave conditions defined in Table 2, and the N of the right *y*-axis indicates the number of cases of each wave age interval. The colors denote different heights. The scale of wave age is logarithmic.

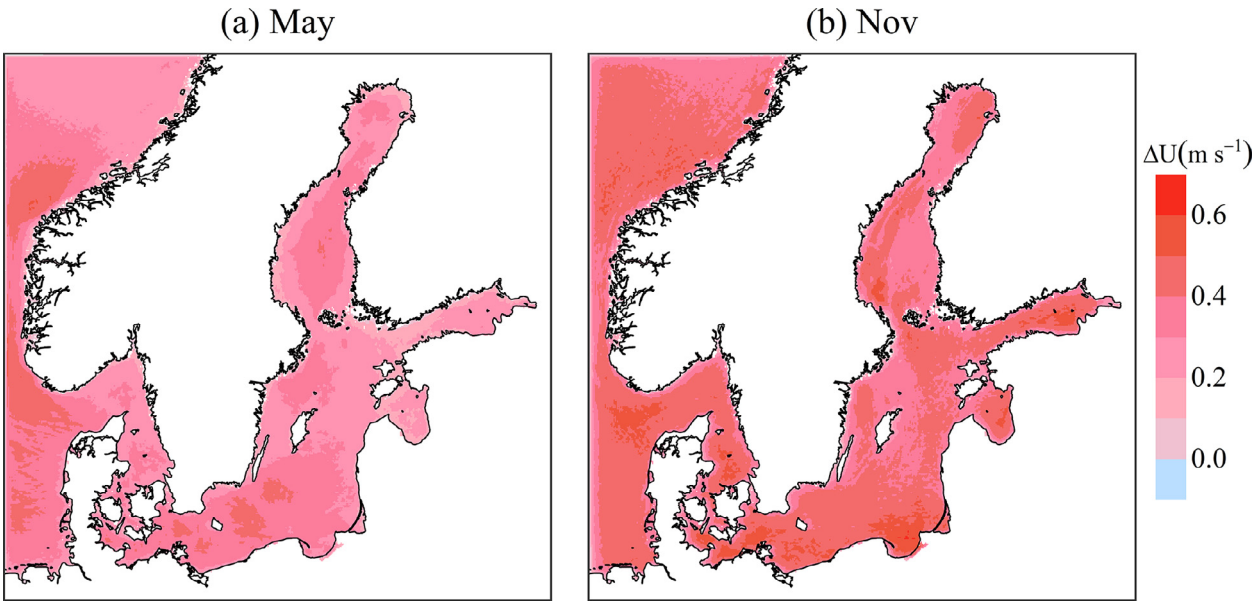

Fig. 11. Difference of monthly mean simulated offshore wind maps at 100 m between run 8 with wave-coupling and 7 without wave-coupling in (a) May and (b) November. The difference less than ±0.01 m s^{-1} is shown in white.

improved the simulated wind over the sea, especially under growing sea and mature wave conditions. The simulations with the finer vertical resolution, updated SST and land surface information only slightly changed the simulated wind under very stable conditions, while simulations with finer horizontal resolution only slightly changed the simulated wind under unstable conditions. To sum up, strengthening the direct forcing from the reanalysis data and atmosphere-wave coupling are promising strategies to improve offshore wind modeling in the study area.

It should be noted that the impact of strengthening direct forcing on the simulated offshore wind largely depends on the accuracy of forcing data. Both our results and a previous study found that the WRF model inherited the general underestimation of the wind speed from ERA5 data and even increased the random errors. This implied that strengthening direct forcing only favored the simulated wind closer to reanalysis data and could not overcome the underestimation in the simulated offshore wind. The accuracy of forcing data needs further improvement for offshore wind modeling. The atmosphere-wave coupling also played an important role in the offshore wind simulation, although we only applied the sea-state-dependent surface roughness length instead of a full coupling. Ocean waves can also affect the wind profile through a wave-induced wind stress profile, which can significantly alter the logarithmic wind profile assumption used in most atmospheric models particularly under swell waves. Besides waves, the underlying ocean can also affect the wind simulation, both directly and indirectly, through atmosphere-wave-ocean interactions, as also shown in some recent studies. Coupling the atmosphere model with both wave and ocean models should be another promising approach to improve offshore wind modeling because they can capture the nonlinear dynamic atmosphere-wave-ocean interactions. Thus, future simulations could consider further improvements on the parameterizations of wave-related coupling processes and coupling with an ocean model. Additionally, increasing the horizontal and vertical resolution, and updating the SST and land surface information also have impacts on the offshore wind modeling under specific conditions or in specific areas and could be taken into consideration if the data are available, even though the overall impact is expected to be small. This study mainly focuses on the sensitivity of short-time wind modeling with a re-initialization to run the model, highlighting the importance of forcing data. The findings may not be applicable for long-term wind modeling which needs further investigation.

Declaration of Competing Interest

The authors declare that they have no known competing financial interests or personal relationships that could have appeared to influence the work reported in this paper.

Acknowledgments

This project was funded by Energimyndigheten [Grant No. 47054-1]. The ICOS station Östergarnsholm is funded by the Swedish Research Council [Grant No. 2012-03902] and Uppsala University. The Finnish Meteorological Institute (FMI) is acknowledged for providing the wave buoy measurements. This work forms part of the Swedish strategic research program StandUp for Wind. L. Wu is supported by Formas project [2017-00516] and Laboratory for Regional Oceanography and Numerical Modeling, Qingdao National Laboratory for Marine Science and Technology [No. 2019B04]. The computations were enabled by resources provided by the Swedish National Infrastructure for Computing (SNIC) at UPPMAX and SMHI partially funded by the Swedish Research Council through grant agreement [No. 2018-05973].

Appendix A. Supplementary data

Supplementary data to this article can be found online at https://doi.org/10.1016/j.gsf.2021.101229.

References

Badger, J., Jørgensen, H.E., 2011. A high resolution global wind atlas-improving estimation of world wind resources. In: Risø International Energy Conference 2011. Danmarks Tekniske Universitet, Risø Nationallaboratoriet for Bæredygtig Energi, pp. 215–225.

Carvalho, D., Rocha, A., Gómez-Gesteira, M., Santos, C., 2012. A sensitivity study of the WRF model in wind simulation for an area of high wind energy. Environ. Model. Softw. 33, 23–34.

Donlon, C.J., Martin, M., Stark, J., Roberts-Jones, J., Fiedler, E., Wimmer, W., 2012. The operational sea surface temperature and sea ice analysis (OSTIA) system. Remote Sens. Environ. 116, 140–158.
Dudhia, J., 1989. Numerical study of convection observed during the winter monsoon experiment using a mesoscale two-dimensional model. J. Atmos. Sci. 46, 3077–3107.
Feranec, J., Jaffrain, G., Soukup, T., Hazeu, G., 2010. Determining changes and flows in European landscapes 1990–2000 using CORINE land cover data. Appl. Geogr. 30 (1), 19–35.
Floors, R., Vincent, C.L., Gryning, S.-E., Peña, A., Batchvarova, E., 2013. The wind profile in the coastal boundary layer: Wind lidar measurements and numerical modelling. Boundary-Layer Meteorol. 147, 469–491.
Floors, R., Enevoldsen, P., Davis, N., Arnqvist, J., Dellwik, E., 2018a. From lidar scans to roughness maps for wind resource modelling in forested areas. Wind Energy Sci 3, 353–370.
Floors, R., Hahmann, A.N., Peña, A., 2018b. Evaluating mesoscale simulations of the coastal flow using lidar measurements. J. Geophys. Res. Atmos. 123 (5), 2718–2736.
Gómez-Navarro, J.J., Raible, C.C., Dierer, S., 2015. Sensitivity of the WRF model to PBL parametrisations and nesting techniques: evaluation of wind storms over complex terrain. Geosci. Model Dev. 8, 3349–3363.
Greene, S., Morrissey, M., Johnson, S.E., 2010. Wind climatology, climate change, and wind energy. Geogr. Compass 4 (11), 1592–1605.
Grell, G.A., Dévényi, D., 2002. A generalized approach to parameterizing convection combining ensemble and data assimilation techniques. Geophys. Res. Lett. 29 (14), 38–1–38–4.
Giannakopoulou, E.-M., Nhili, R., 2014. WRF model methodology for offshore wind energy applications. Adv. Meteorol., 319819 https://doi.org/10.1155/2014/319819.
Hahmann, A.N., Vincent, C.L., Peña, A., Lange, J., Hasager, C.B., 2015. Wind climate estimation using WRF model output: method and model sensitivities over the sea. Int. J. Climatol. 35, 3422–3439.
Hahmann, A.N., Sīle, T., Witha, B., Davis, N.N., Dörenkämper, M., Ezber, Y., García-Bustamante, E., González-Rouco, J.F., Navarro, J., Olsen, B.T., Söderberg, S., 2020. The making of the new european wind atlas–part 1: Model sensitivity. Geosci. Model Dev. 13 (10), 5053–5078.
Hallgren, C., Arnqvist, J., Ivanell, S., Körnich, H., Vakkari, V., Sahlée, E., 2020. Looking for an offshore low-level jet champion among recent reanalyses: A tight race over the Baltic Sea. Energies 13, 3670. https://doi.org/10.3390/en13143670.
Hersbach, H., Bell, B., Berrisford, P., Hirahara, S., Horányi, A., Muñoz-Sabater, J., Nicolas, J., Peubey, C., Radu, R., Schepers, D., 2020. The ERA5 global reanalysis. Q. J. Roy. Meteorol. Soc. 146, 1999–2049.
Holtslag, A.A.M., Svensson, G., Baas, P., Basu, S., Beare, B., Beljaars, A.C.M., Bosveld, F. C., Cuxart, J., Lindvall, J., Steeneveld, G.J., Tjernström, M., 2013. Stable atmospheric boundary layers and diurnal cycles: Challenges for weather and climate models. Bull. Amer. Meteorol. Soc. 94, 1691–1706.
Högström, U., Sahlée, E., Smedman, A.-S., Rutgersson, A., Nilsson, E., Kahma, K.K., Drennan, W.M., 2018. The transition from downward to upward air–sea momentum flux in swell-dominated light wind conditions. J. Atmos. Sci. 75, 2579–2588.
Högström, U., Sahlée, E., Smedman, A.S., Rutgersson, A., Nilsson, E., Kahma, K.K., Drennan, W.M., 2015. Surface stress over the ocean in swell-dominated conditions during moderate winds. J. Atmos. Sci. 72, 4777–4795.
Høyer, J.L., She, J., 2007. Optimal interpolation of sea surface temperature for the North Sea and Baltic Sea. J. Mar. Syst. 65 (1–4), 176–189.
Janssen, P.A.E.M., 1989. Wave-induced stress and the drag of air flow over sea waves. J. Phys. Oceanogr. 19 (6), 745–754.
Kalverla, P., Steeneveld, G.-J., Ronda, R., Holtslag, A.AM., 2019. Evaluation of three mainstream numerical weather prediction models with observations from meteorological mast IJmuiden at the North Sea. Wind Energy 22, 34–48.
Kalverla, P.C., Holtslag, A.A.M., Ronda, R.J., Steeneveld, G.-J., 2020. Quality of wind characteristics in recent wind atlases over the North Sea. Q. J. R. Meteorol. Soc. 146, 1498–1515.
Kalvig, S., Gudmestad, O.T., Winther, N., 2014. Exploring the gap between 'best knowledge'and 'best practice'in boundary layer meteorology for offshore wind energy. Wind Energy 17, 161–171.
Karagali, I., Hahmann, A.N., Badger, M., Hasager, C., Mann, J., 2018. New European wind atlas offshore. J. Phys. Conf. Ser. 1037, 52007.
Lantmäteriet, 2020. GSD-Elevation data, grid 50+ nh. https://www.lantmateriet.se/globalassets/kartor-och-geografisk-information/hojddata/hojd50_plus_nh_v1.2.pdf.
Larsén, X.G., Du, J., Bolaños, R., Imberger, M., Kelly, M.C., Badger, M., Larsen, S., 2019. Estimation of offshore extreme wind from wind-wave coupled modeling. Wind Energy 22 (8), 1043–1057.
Li, H., Wolter, M., Wang, X., Sodoudi, S., 2018. Impact of land cover data on the simulation of urban heat island for Berlin using WRF coupled with bulk approach of Noah-LSM. Theor. Appl. Climatol. 134, 67–81.
Li, H., Sodoudi, S., Liu, J., Tao, W., 2020. Temporal variation of urban aerosol pollution island and its relationship with urban heat island. Atmos. Res. 241, 104957. https://doi.org/10.1016/j.atmosres.2020.104957.
Mlawer, E.J., Taubman, S.J., Brown, P.D., Iacono, M.J., Clough, S.A., 1997. Radiative transfer for inhomogeneous atmospheres: RRTM, a validated correlated-k model for the longwave. J. Geophys. Res. Atmos. 102, 16663–16682.
Murthy, K.S.R., Rahi, O.P., 2017. A comprehensive review of wind resource assessment. Renew. Sustain. Energy Rev. 72, 1320–1342.
Nakanishi, M., Niino, H., 2009. Development of an improved turbulence closure model for the atmospheric boundary layer. J. Meteorol. Soc. Japan. Ser. II 87, 895–912.
Nunalee, C.G., Basu, S., 2014. Mesoscale modeling of coastal low-level jets: implications for offshore wind resource estimation. Wind Energy 17, 1199–1216.
Olsen, B.T., Hahmann, A.N., Sempreviva, A.M., Badger, J., Jørgensen, H.E., 2017. An intercomparison of mesoscale models at simple sites for wind energy applications. Wind Energy Sciences 2 (1), 211–228.
Pineda, N., Jorba, O., Jorge, J., Baldasano, J.M., 2004. Using NOAA AVHRR and SPOT VGT data to estimate surface parameters: application to a mesoscale meteorological model. Int. J. Remote Sens. 25, 129–143.
Qiao, W., Wu, L., Song, J., Li, X., Qiao, F., Rutgersson, A., 2021. Momentum flux balance at the air-sea interface. J. Geophys. Res. Oceans 126. e2020JC016563.
Rutgersson, A., Pettersson, H., Nilsson, E., Bergström, H., Wallin, M.B., Nilsson, E.D., Sahlée, E., Wu, L., Mårtensson, E.M., 2020. Using land-based stations for air–sea interaction studies. Tellus. Ser. A Dyn. Meteorol. Oceanogr. 72, 1–23.
Sanz Rodrigo, J., Chávez Arroyo, R.A., Moriarty, P., Churchfield, M., Kosović, B., Réthoré, P.-E., Hansen, K.S., Hahmann, A., Mirocha, J.D., Rife, D., 2017. Mesoscale to microscale wind farm flow modeling and evaluation. Wiley Interdiscip. Rev. Energy Environ. 6 (2), e214.
Santos-Alamillos, F.J., Pozo-Vázquez, D., Ruiz-Arias, J.A., Lara-Fanego, V., Tovar-Pescador, J., 2013. Analysis of WRF model wind estimate sensitivity to physics parameterization choice and terrain representation in Andalusia (Southern Spain). J. Appl. Meteorol. Climatol. 52, 1592–1609.
Sproson, D., Sahlée, E., 2014. Modelling the impact of Baltic Sea upwelling on the atmospheric boundary layer. Tellus. Ser. A Dyn. Meteorol. Oceanogr. 66, 24041. https://doi.org/10.3402/tellusa:v66.24041.
Svensson, N., Bergström, H., Sahlée, E., Rutgersson, A., 2016. Stable atmospheric conditions over the Baltic Sea: model evaluation and climatology. Boreal Environ. Res. 21, 387–404.
Svensson, N., Bergström, H., Rutgersson, A., Sahlée, E., 2019a. Modification of the Baltic Sea wind field by land-sea interaction. Wind Energy 22, 764–779.
Svensson, N., Arnqvist, J., Bergström, H., Rutgersson, A., Sahlée, E., 2019b. Measurements and modelling of offshorewind profiles in a Semi-Enclosed Sea. Atmosphere 10 (4), 194.
Tewari, M., Chen, F., Wang, W., Dudhia, J., LeMone, M.A., Mitchell, K., Ek, M., Gayno, G., Wegiel, J., Cuenca, R.H., 2004. Implementation and verification of the unified NOAH land surface model in the WRF model. In: 20th Conference on Weather Analysis and Forecasting/16th Conference on Numerical Weather Prediction. American Meteorological Society, Seattle, WA.
Thompson, G., Field, P.R., Rasmussen, R.M., Hall, W.D., 2008. Explicit forecasts of winter precipitation using an improved bulk microphysics scheme. Part II: Implementation of a new snow parameterization. Mon. Weather Rev. 136, 5095–5115.
Valcke, S., Craig, T., Coquart, L., 2013. OASIS3-MCT user guide, oasis3-mct 2.0. Toulouse, France.
Veers, P., Dykes, K., Lantz, E., Barth, S., Bottasso, C.L., Carlson, O., Clifton, A., Green, J., Green, P., Holttinen, H., Laird, D., Lehtomäki, V., Lundquist, J.K., Manwell, J., Marquis, M., Meneveau, C., Moriarty, P., Munduate, X., Muskulus, M., Naughton, J., Pao, L., Paquette, J., Peinke, J., Robertson, A., Sanz Rodrigo, J., Sempreviva, A.M., Smith, J.C., Tuohy, A., Wiser, R., 2019. Grand challenges in the science of wind energy. Science 366, 1–8.
Wu, L., Rutgersson, A., Sahlée, E., Guo Larsén, X., 2016. Swell impact on wind stress and atmospheric mixing in a regional coupled atmosphere-wave model. J. Geophys. Res. Ocean. 121, 4633–4648.
Wu, L., Rutgersson, A., Nilsson, E., 2017. Atmospheric boundary layer turbulence closure scheme for wind-following swell conditions. J. Atmos. Sci. 74, 2363–2382.
Wu, L., Breivik, Ø., Rutgersson, A., 2019. Ocean-wave-atmosphere interaction processes in a fully coupled modeling system. J. Adv. Model. Earth Syst. 11, 3852–3874.
Wu, L., Shao, M., Sahlée, E., 2020. Impact of air–wave–sea coupling on the simulation of offshore wind and wave energy potentials. Atmosphere 11, 327. https://doi.org/10.3390/atmos11040327.
Zheng, C.W., Li, C.Y., Pan, J., Liu, M.Y., Xia, L.L., 2016. An overview of global ocean wind energy resource evaluations. Renew. Sustain. Energy Rev. 53, 1240–1251.
Zhou, X., Qin, J., Li, H.D., Tang, W., Pan, X., Huang, B., Li, X., 2020. A statistical method to construct wind speed at turbine height for study of wind power in China. Theor. Appl. Climatol. 141, 419–432.
SWEA (Swedish Wind Energy Association). 100 percent renewable electricity by 2040-wind power: combating climate change and improving competitiveness. 2019. https://swedishwindenergy.com/wp-content/uploads/2019/10/Svensk_Vindenergi_ROADMAP_2040_rev_ENG-1.pdf.